JOURNAL OF THERMOPHYSICS AND HEAT TRANSFER
Vol. 17, No. 3, July–September 2003

Heat-Transfer Analysis in Heat Sink Embedded with a Thermosyphon

C. K. Teoh,* M. R. Maschmann,* and H. B. Ma†
University of Missouri—Columbia, Columbia, Missouri 65203

A mathematical model for predicting the heat-transfer performance in a heat sink embedded with a closed two-phase thermosyphon is presented. The model includes boiling heat transfer in the evaporator, vapor flow influence on condensation heat transfer, and the effects of fin surface areas and airflow rates on the convection heat transfer. The results obtained from the model indicate that the heat-transfer resistance occurring in the evaporator is the primary factor affecting the total temperature drop in the heat sink embedded with a thermosyphon. Although the effect of vapor flow on the condensation heat transfer can be neglected, the condensation heat transfer in the condenser significantly depends on the type of working fluid. In addition, a new relationship between heat transfer and flow characteristics in terms of the Colburn factor j_H and the Reynolds number was developed to predict the forced airflow effect on the fin-tube condenser's heat-transfer performance. A correlation for boiling heat transfer occurring in the evaporator was also determined experimentally. To verify the prediction, an experimental investigation was conducted to measure the temperature drops from the evaporator to the forced airflow in the heat sink embedded with a thermosyphon charged with acetone. The results of this investigation will assist in the development of high heat-flux cooling devices capable of operating at power levels up to 120 W/cm^2 with a low temperature drop.

Nomenclature

A = area, m^2
c_p = specific heat, J/kg-K
D = hydraulic diameter, m
f = friction factor
G = maximum flow rate, kg/m^2-s
g = gravitational acceleration, m/s^2
h = heat-transfer coefficient, W/m^2-K
h_{fg} = latent heat of evaporation, J/kg
j_H = Colburn factor
k = thermal conductivity, W/m-K
L = length, m
$\dot{m}$ = mass flow rate, kg/s
N = number of fins
P = perimeter, m
Pr = Prandtl number
p = pressure, N/m^2
Q = heat transfer, W
q'' = heat flux, W/m^2
Re = Reynolds number
St = Stanton number
T = temperature, K
u = velocity, m/s
V = volume, m^3
w = width of vapor channel, m
x = coordinate
δ = film thickness, m
η = fin efficiency
μ = dynamic viscosity, N-s/m^2
ρ = mass density, kg/m^3
σ = surface tension, N/m
ψ = tilt angle

Subscripts

a = air
b = base, boiling
c = condensate, cross-sectional
e = evaporator
f = fin
ff = free flow
ft = frontal
h = flow passage
i = inner
l = liquid
m = mean vapor
s = shell
sat = saturation
t = total
v = vapor
w = wall

Received 25 April 2002; revision received 13 November 2002; accepted for publication 10 January 2003.

*Graduate Research Assistant, Department of Mechanical and Aerospace Engineering.

†Assistant Professor, Department of Mechanical and Aerospace Engineering; mah@missouri.edu. Member AIAA.

Introduction

THE earliest literature on the two-phase closed thermosyphon was recorded in 1955 for turbine blade cooling.[1] Since then, thermosyphons have been used in a variety of applications including preservation of permafrost,[2,3] de-icing of roadways,[4,5] heat exchangers,[6,7] and power reactor cooling.[8] A thermosyphon is an entirely passive, enclosed system utilizing liquid–vapor phase change of an internal working fluid to dissipate heat, which has been systematically investigated including the boiling limit,[9–11] flooding limit,[12–20] vapor flow effect,[12,16–20] and oscillating motions.[21–24] These investigations have provided insights into the heat-transfer mechanisms and led to a better understanding of operating limits occurring in a thermosyphon.

Although these investigations have pushed the application boundary of thermosyphons, most of these applications were limited to low heat fluxes. In addition, as the heat-flux level increases to higher than, for example, 1.0 MW/m^2, the thermosyphon might not reach these traditional limits. The temperature drop produced in the device might exceed the requirement for proper functionality. Clearly, it is necessary to conduct a detailed analysis of heat transfer in a heat sink embedded with a thermosyphon, particularly for high heat-flux applications. In the current investigation a heat sink embedded with a thermosyphon was analyzed and tested to determine the primary factors affecting the heat-transfer performance.

Theoretical Analysis

Figure 1 illustrates a heat sink embedded with a thermosyphon, which consists of an evaporator and a four-tube condenser. As heat is applied on the evaporator from a heat source, it is transferred via conduction across the evaporator shell, evaporation in the evaporator, vapor flow from the evaporator to the condenser, condensation in the condenser, and finally conduction and convection from the condenser wall through the fin surface and to the forced airflow. In the following analysis a detailed model describing the heat transfer in the individual sections will be presented.

Heat Transfer in the Evaporator

As heat is transferred across the evaporator shell and reaches the working fluid, evaporation occurs at the solid–liquid interface if the solid surface temperature exceeds the saturation temperature corresponding to the local pressure, which can be expressed as

$$q_e'' = h_b \Delta T_e \tag{1}$$

where $\Delta T_e = T_{e,w} - T_{e,\text{sat}}$. The boiling heat-transfer coefficient h_b shown in Eq. (1) is characterized by the formation of vapor bubbles, which directly depends on the applied heat-flux level, surface conditions, thermophysical properties of the working fluid, and the superheat ΔT_e. In addition, the following features were found from the experimental observation on the thermosyphon shown in Fig. 1: 1) the critical heat flux predicted by the well-known equation developed by Zuber[25] was lower than the maximum heat flux applied in the testing, and 2) there was no sign that the evaporator experienced dryout.

To determine the best model for predicting the boiling heat transfer occurring in the evaporator shown in Fig. 1, equations developed by Jacob and Linke,[26] Rohsenow,[27] and Foster and Zuber[28] were evaluated. Comparison with the experimental data showed that preceding correlations poorly predicted the heat transfer occurring in the evaporator investigated herein. However, the correlation

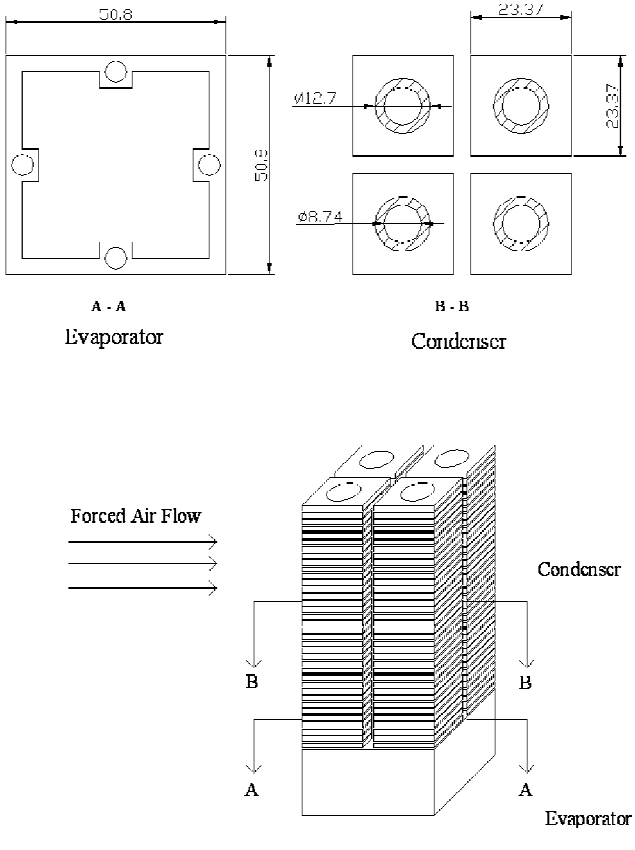

Fig. 1 Schematic of the heat sink embedded with a thermosyphon (millimeters).

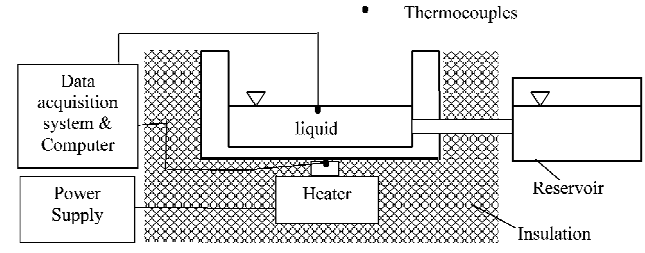

Fig. 2 Setup for determining constants in Eq. (2).

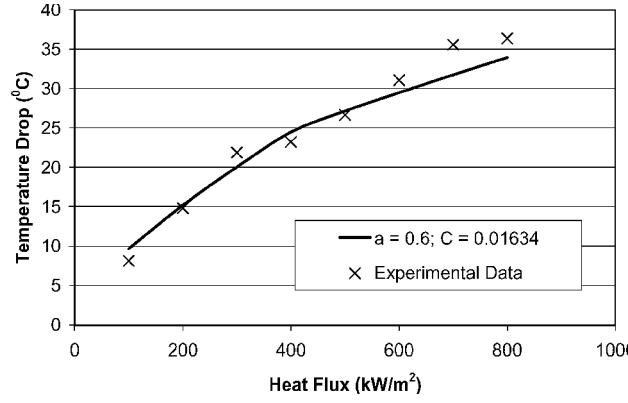

Fig. 3 Boiling heat transfer in the evaporator.

developed by Forster and Zuber,[28] that is,

$$q_e'' = C\left(\frac{k_l^{0.79} c_{\text{pl}}^{0.45} \rho_l^{0.49}}{\sigma^{0.5} \mu_l^{0.29} h_{\text{fg}}^{0.24} \rho_v^{0.24}}\right)(T_{e,w} - T_{e,\text{sat}})^a \Delta P_{\text{sat}}^{0.75} \tag{2}$$

presented a trend similar to the experimental data. In practice, the constants, that is, C and a, shown in Eq. (2), can be modified to fit the experimental data, and Eq. (2) can be used to predict the superheat as a function of heat flux occurring in the evaporator.

To determine these constants, an experimental system shown in Fig. 2 was established, consisting of a heater, an evaporator, a reservoir, a working fluid, and a data acquisition system. Two thermocouples were used to measure the temperature difference between the evaporator shell and the liquid temperature. The evaporator was well insulated during testing to minimize heat loss to the surrounding. The detailed experimental procedure, including the experimental error, is discussed later in the section Experimental System and Procedure. The experimental data showed that surface-temperature variation closely followed the nucleate boiling curve, and it was therefore determined that nucleate boiling is the dominant boiling mechanism occurring in the evaporator over the heat-flux ranges experimentally tested. Comparison with the experimental data indicates that the constants of C and a are equal to 0.01634 and 0.6, respectively. The correlation is shown in Fig. 3.

Heat Transfer in the Condenser

As the vapor generated in the evaporator flows into the condenser, vapor condenses into liquid and forms a condensate film, as shown in Fig. 4a. Because of the gravitational force, the condensate flows downward. The condensing film thickness and the mass flow rate increase with increasing x because of continuous condensation at the liquid–vapor interface throughout the total length. Following a derivation similar to the Nusselt analysis, the x-momentum equation for the condensate flow can be written as

$$\frac{\partial^2 u_l}{\partial y^2} = \frac{1}{\mu_l}\left(\frac{\mathrm{d}p_v}{\mathrm{d}x} - \rho_l g\right) \tag{3}$$

As shown in Fig. 4a, the vapor flow in the thermosyphon is counter to the condensate flow direction. The shear stress occurring at the

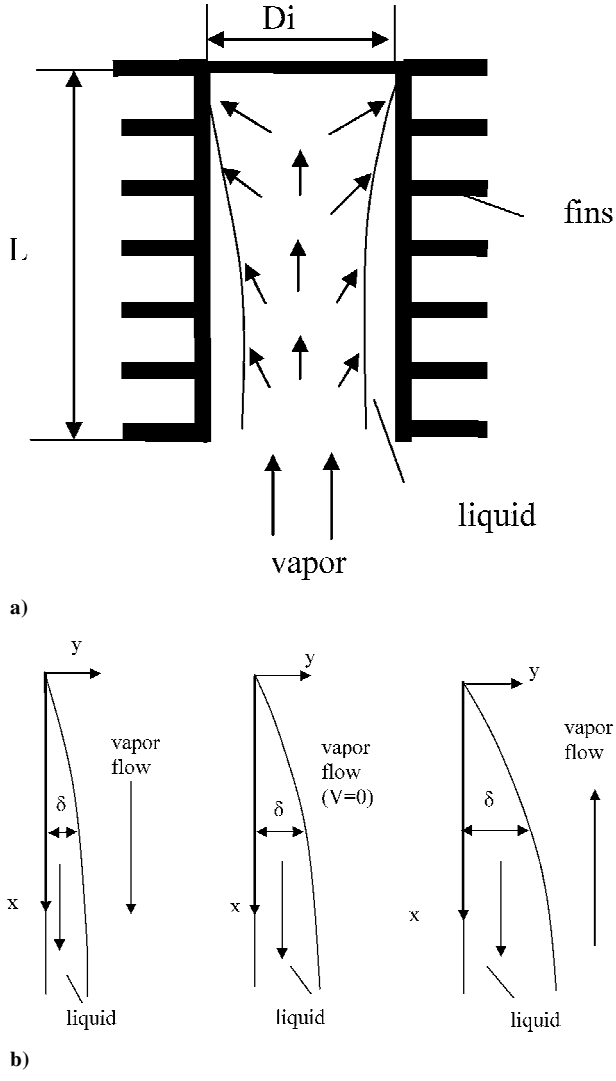

Fig. 4 Vapor flow effect on the condensation film.

liquid–vapor interface will affect the condensate film thickness, leading to the following boundary condition:

$$\left.\frac{\mathrm{d}u_l}{\mathrm{d}y}\right|_{y=\delta} = \frac{D_i}{4\mu_l}\left(\frac{\mathrm{d}p_v}{\mathrm{d}x}\right) \quad \text{at} \quad y = \delta \tag{4}$$

for Eq. (3). The vapor pressure drop caused by the effect of frictional vapor flow on the liquid–vapor interface shown in Eqs. (3) and (4) can be found by the following:

$$\frac{\mathrm{d}p_v}{\mathrm{d}x} = \frac{-f_v \cdot Re_v \mu_v u_m}{2D_i^2} \tag{5}$$

$$\frac{\mathrm{d}p_v}{\mathrm{d}x} = \frac{f_v \cdot Re_v \mu_v u_m}{2D_i^2} \tag{6}$$

for parallel flows and counterflows, respectively. If the vapor flow direction is the same as the condensate flow direction, the condensate film thickness will become thinner and enhance the condensing heat transfer, as shown in Fig. 4b. Considering a no-slip boundary condition at the condenser wall, Eq. (3) can be readily solved for the condensate velocity distribution. Based on mass and energy conservation, the equation governing the condensate thickness δ can be found as

$$\frac{\mathrm{d}\delta}{\mathrm{d}x} = \frac{k_l \mu_l \Delta T_c}{h_{\mathrm{fg}} \rho_l^2 \delta^3 - (\mathrm{d}p_v/\mathrm{d}x)(\delta^3 + D_i \delta^2/4)} \tag{7}$$

where $\Delta T_c = T_{c,\mathrm{sat}} - T_{c,w}$. Equation (7) is based on the assumption of laminar condensate flow.

As shown in Eqs. (4–7), the velocity distribution of vapor flow must be obtained prior to solving Eq. (7). Because of the condensation film thickness variation with vertical height, as shown in Fig. 4a, the vapor space decreases with increasing x. The decrease in condensing rate with increasing film thickness directly affects the boundary conditions of vapor flow at the liquid–vapor interface. For a round vapor flow channel the friction factor and Reynolds-number product are constant for a developed laminar flow and will not depend on the hydraulic diameter of the vapor flow channel. Once the friction factor is obtained, the one-dimensional momentum equation for vapor flow along the x direction can be expressed as

$$\frac{\mathrm{d}p_v}{\mathrm{d}x} + \rho_v g \sin\psi + \rho_v u_m \frac{\mathrm{d}u_m}{\mathrm{d}x} = -f_v \frac{2\rho_v u_m^2}{D_i} \tag{8}$$

where $f_v = 64/Re_v$. Because of the frictional vapor flow, the vapor pressure varies from the inlet of the condenser to the cap end of the condenser. For a given condensation rate along the condensing surface, the boundary conditions for the vapor flow are established, and the velocity at a given location can be determined. Once the vapor pressure drop is calculated from Eq. (8), Eq. (7) can be solved for the condensation film thickness, and the local heat-transfer coefficient and temperature drop across the condensate liquid film can be readily determined.

In addition, the pressure drop in the vapor flow results in the temperature variation as a result of the saturated vapor flow. Based on the Clapeyron equation, the vapor temperature variation can be found as

$$\Delta T_v = T_{e,\mathrm{sat}} - T_{c,\mathrm{sat}} = [T(1/\rho_l - 1/\rho_v)/h_{\mathrm{fg}}]\Delta p_v \tag{9}$$

Because the pressure drop in the vapor flow is very small, the temperature drop in the vapor flow can be neglected in comparison with the temperature drops occurring in the condenser, evaporator, and fins.

When transferred to the condensing wall, heat is distributed across the fins through conduction and removed by the forced convection. Based on the energy balance, the governing equation describing the temperature distribution on the fins can be readily found and solved for a given convection coefficient. The total heat transfer from the base and fin surfaces can be determined as follows:

$$Q = h_f[N\eta_f A_f + (A_t - NA_f)]\Delta T_f \tag{10}$$

where $\Delta T_f = T_{c,w} - T_\infty$. Because the fin thickness is very small, the heat transfer through fin tip areas can be neglected. The heat-transfer rate through a single fin can be found as

$$q_f = \sqrt{h_f P k A_c}\,\Delta T_f \tag{11}$$

As shown in Eq. (10), the heat-transfer coefficient h_f is a key for determining the heat transfer through the fins. For the fins shown in Fig. 1, it is difficult to obtain an analytical solution for the convection coefficient. Kays and London[29] showed that the convection coefficient for the tube fins similar to one shown in Fig. 1 can be expressed as

$$h_f = j_H G c_p Pr^{-\frac{2}{3}} \tag{12}$$

where the value of Colburn factor j_H can be determined by experimental investigation.

Experimental System and Procedures

The heat sink embedded with a thermosyphon investigated here was fabricated from aluminum 6061-T6. As shown in Fig. 1, it consists of an evaporator and a four-tube condenser charged with acetone. Each tube was aligned with total of 35 square fins (23.37×23.37 mm). In addition, a charging nozzle was brazed on one of the condenser tubes for charging the thermosyphon. The heat

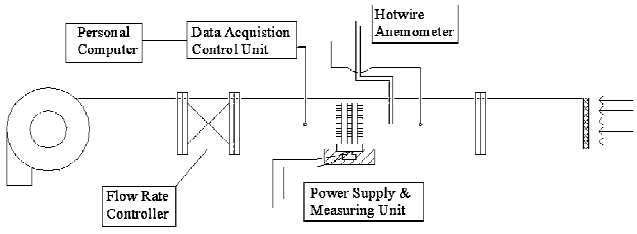

Fig. 5 Schematic of the experimental setup.

added on the evaporator was transferred through the evaporator to the condenser via vapor, where the heat was removed by the fins through forced convection.

To test the heat sink embedded with a thermosyphon, an experimental system, as shown in Fig. 5, was established, consisting of a wind tunnel, a blower, a data acquisition unit, a hot-wire anemometer, a power supply and measurement unit, and a PC. The wind tunnel was fabricated from Lexan sheets. An opening was constructed in the wind tunnel so that the thermosyphon could be positioned in such a way that only finned regions were exposed to the airstream. A blower was used to create the forced airflow, and the flow rate was controlled by an adjustable opening located downstream from the thermosyphon. A hot-wire anemometer probe was employed to measure the airflow velocity. Two thermocouples were placed at the inlet and outlet of the wind tunnel to monitor the air temperature variation, which were also used to verify the heat input. Four thermocouples were mounted in four microgrooves specially manufactured at the base of the evaporator in order to accurately measure the base temperature. Seven thermocouples were mounted on the external surface of each condenser tube wall. All thermocouples were made of AWG-36 Copper-Constantan wires with a full-scale error of 0.75%. To reduce the influence of the thermocouple wires on the airflow, the thermocouples were placed on the two tubes positioned downstream. Omegabond 200 was used to bond all thermalcouples. All of the thermocouples were monitored using an IO/Tech Personal DAQ56 data acquisition system controlled by a personal computer. Heat was added on the evaporator through a 2.54-cm-diam copper block, wrapped by a heating coil (FAST HEAT BB010002, 200W, 120 V). The heater cross-sectional area contacting with the evaporator was machined to be 1×1 cm^2 to simulate an electronic chip. The heater was insulated in order to diminish the heat loss. At the contact surface between the heater and the evaporator, high thermal conductivity paste (OMEGATHERMA "201") was used to minimize contact resistance between the heater and the evaporator wall. The desired power input was obtained by adjusting the voltage applied to the heating coil.

Before the thermosyphon was charged, the interior portion of the thermosyphon was cleaned thoroughly. The existence of any particles on the inside surface would result in chemical reactions and produce noncondensable gases. The evacuation and backfilling technique[30] was employed to charge the exact amount of working fluid. Prior to the start of the experiment, the system was allowed to equilibrate and reach steady state. When the steady-state condition had been obtained, the input power was increased in small increments. Experimental data indicated that a time of approximately 30 minutes was necessary to achieve the steady state. To obtain the data for the next successive power level, the power was incremented every 30 minutes. During the tests, the input power and temperature data, including the ambient temperature, were simultaneously recorded through the data acquisition system.

As just illustrated, four fine thermocouples were bonded on the microgrooves specially designed for temperature measurements, which could significantly reduce the effect of contact resistance on the uniform heat-flux condition. However, a temperature difference of $\pm 2.5^\circ$C for the highest power of 800 kW/m^2 still existed among these four thermocouples as a result of the nonuniform thickness of Omegabond adhesive between the thermocouples and the evaporator wall. Ambient temperature was obtained by measuring the inlet airflow temperature, which was approximately $24 \pm 0.5^\circ$C. The steady-state condition was defined as the temperature for which less than 1 deg of change was observed for 5 minutes of continuously applied heat. Although the test section and heater were well insulated, some heat losses caused by the combined effects of radiation, conduction, and convection were inevitable. Calculations for the amount of heat loss based on outer insulation temperatures indicated that the loss was less than 5% of the total heat added on the heater. Combining the temperature measurement errors, the total measurement errors were less than $\pm 6\%$.

Results and Discussion

As just described, the value of Colburn factor j_H, shown in Eq. (12), depends on the specific design of the fins. For the circular tube-square fin condenser shown in Fig. 1, the Colburn j_H factor, that is, $j_H = St\,Pr^{2/3}$, only depends on the Reynolds number, where the Stanton and Reynolds number are defined as

$$St = h_f / G c_p \tag{13}$$

$$Re_a = G D_h / \mu_a \tag{14}$$

respectively. The Stanton and Reynolds number, as shown in Eqs. (13) and (14), are based on the maximum air velocity, that is, $G = \rho_a V_{a,\max} = \rho_a V_a / \sigma$, where σ is defined as the ratio of the free-flow area to the frontal area, that is, $\sigma = A_{\text{ff}}/A_{\text{ft}}$. Considering Eqs. (13) and (14), Eq. (12) can be rewritten as

$$j_H = \frac{h_f Pr^{\frac{2}{3}} D_{a,h}}{Re_a c_p \mu_a} \tag{15}$$

where the convection coefficient h_f can be experimentally determined. Based on the air properties at the temperature of 24°C and dimensions shown in Table 1, the Colburn j_H factor can be readily found, and results are shown in Fig. 6.

To verify the model presented in the paper, experimental measurements were made, and the results are presented in terms of the temperature drop from the evaporator to the forced airflow, that is, ΔT_t, and the heat transport Q. The total temperature drop was calculated by summing the temperature drop of each heat transport process, that is, conduction across the evaporator shell ΔT_s, boiling heat transfer in the evaporator ΔT_e, vapor pressure effect on the temperature drop in the vapor flow ΔT_v, condensation heat transfer

Table 1 Dimensions of the tube-fin condenser

Names	Dimensions
Tube outside diameter	12.7 mm
Fin pitch	416 per meter
Flow passage hydraulic diameter, D_h	2.961 mm
Fin thickness	0.6 mm
Free-flow area/frontal area, σ	0.4
Heat-transfer area/total volume, α	593 m^2/m^3
Fin area/total area, A_f/A_t	0.920

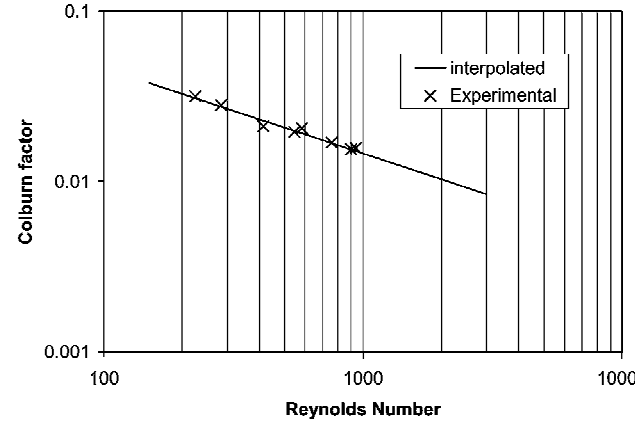

Fig. 6 Relationship between Colburn *jH* factor and Reynolds number.

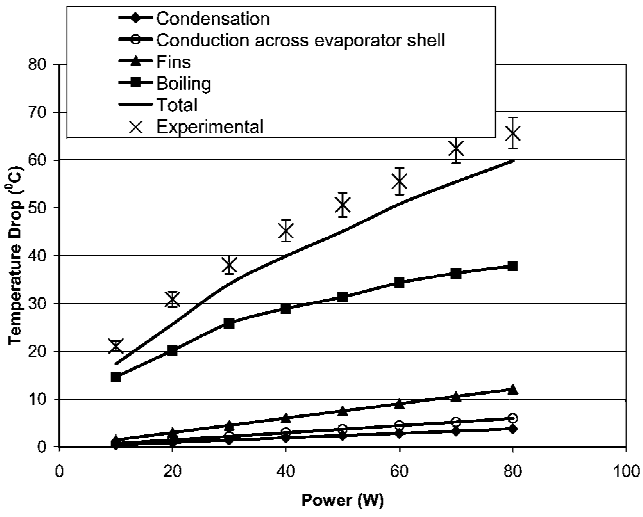

Fig. 7 Comparison with experimental results.

in the condenser ΔT_c, and conduction and convection from the condenser wall through the fin surface to the forced airflow ΔT_f, that is,

$$\Delta T_t = \Delta T_s + \Delta T_e + \Delta T_v + \Delta T_c + \Delta T_f \tag{16}$$

The total temperature drop including the contributions of each temperature drop calculated from Eq. (16) are plotted in Fig. 7. As shown, the prediction agrees well with the experimental data. Results indicate that the temperature drop caused by the boiling heat-transfer resistance in the evaporator is the primary contribution to the total temperature drop. The temperature drop in the vapor flow can be neglected. The prediction considered the effect of surface roughness on the condensation heat transfer. The inside surface of condenser tube was analyzed with the surface roughness detector, and it was found that the surface roughness for the condenser surface was approximately $13.2 \pm 0.5\ \mu$. The effect of surface roughness on the condensation film thickness was considered by adding an additional film thickness δ_r to each film thickness value. Because Eq. (2) for the boiling heat transfer in the evaporator was determined at the atmospheric pressure and a constant liquid level, there exists a deviation between the experimental data and prediction when Eq. (2) is used to predict the temperature drop occurring in the closed two-phase thermosyphon where the liquid level and saturated pressure depended on the power input.

As shown in Fig. 4a, the vapor flow direction is different from the condensate flow. The shear stress acting on the liquid–vapor interface by the frictional vapor flow will drag the condensate and produce the additional liquid pressure drop for returning the condensate back to the evaporator. If the vapor flow direction is the same as the condensate flow, the frictional vapor flow will help the condensate flow, as visualized in Fig. 4b. Figure 8 illustrates the effect of vapor flow direction on the condensation heat transfer and indicates that when the input power was less than 120 W the effect of vapor flow can be neglected for the thermosyphon investigated herein. When the power is increased or the condensing area is reduced, the vapor flow effect on the temperature drop becomes significant and should be considered in the model. In addition, when the input power increases the condensing rate, film thickness, and the film Reynolds number $[Re_\delta = 4g\rho_l(\rho_l - \rho_v)\delta^3/3\mu_l^2]$ increase. Figure 9 illustrates the effect of input power on the film thickness variation along the x direction. And the film Reynolds number Re_δ at the location of $x = L$ indicates that the assumption of laminar flow is valid as the input power is less than 150 W for the thermosyphon investigated herein.

Although it is demonstrated that the vapor flow has little effect on the condensate film thickness for the thermosyphon charging with acetone, the temperature drop across the condensate film is significantly dependent on the working fluid. As shown in Fig. 10,

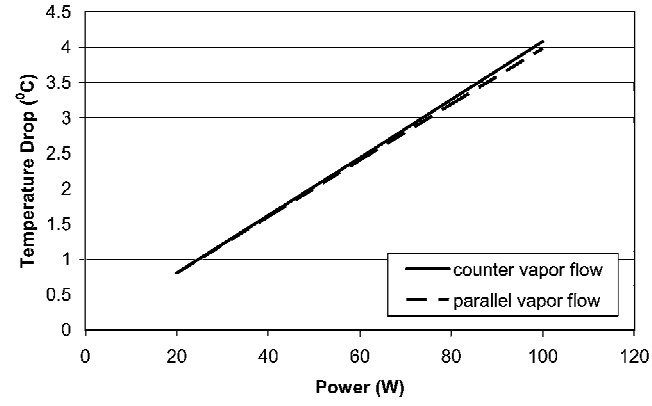

Fig. 8 Vapor flow effect on the temperature drop of condensation film.

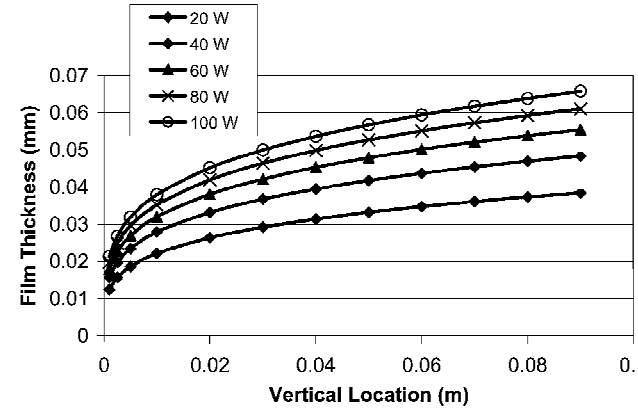

Fig. 9 Condensation film thickness variation along the x direction.

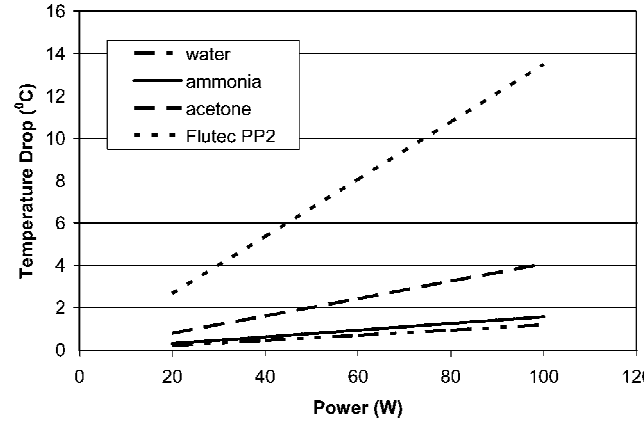

Fig. 10 Effect of working fluids on the temperature drop of condensation film.

water was predicted to have the lowest temperature drop and Flutec PP2 the highest among working fluids investigated. It is found that the latent heat of vaporization and thermal conductivity of working fluid significantly affect the condensation heat transfer in the thermosyphon investigated herein. All of the properties are evaluated at the operating temperature of 40°C.

Figure 11 illustrates the effect of the total fin surface area on the temperature drop occurring in the forced convection. As shown, when the total fin surface area, indicated by the ratio of the total surface area to the total volume, that is, α, increases from 184 to 730 m^2/m^3, the temperature drop occurring in the forced convection is significantly reduced. However, the further increase of the fin surface area would not significantly enhance the heat transfer for the thermosyphon investigated herein. Of course, the total temperature drop depended on the forced airflow rate. As shown in Fig. 12, the increase of forced airflow rate will enhance heat transfer.

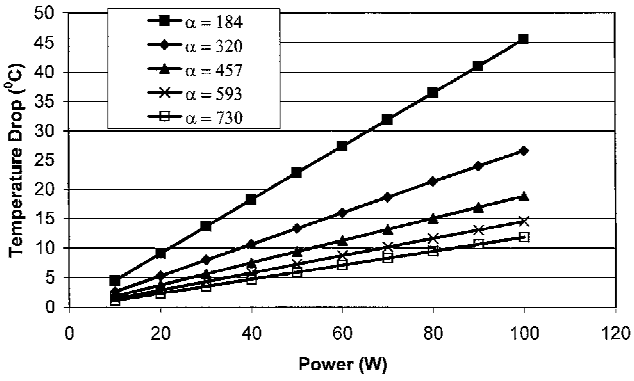

Fig. 11 Effect of fin surface area on the temperature drop of fins.

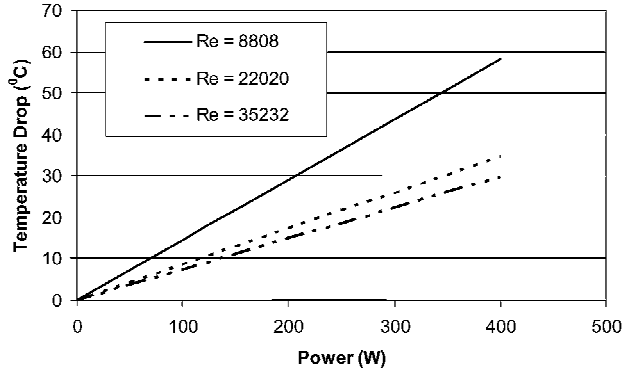

Fig. 12 Effect of airflow velocity on the temperature drop of fins.

Conclusions

A mathematical model predicting the heat transfer in a heat sink embedded with a thermosyphon was developed. The model includes boiling heat transfer in the evaporator, vapor flow influence on condensation heat transfer, and the effects of fin surface areas and airflow rates on the convection heat transfer. The heat-transfer analysis is presented in terms of the temperature drop from the evaporator to the forced airflow as a function of the heat input. The results obtained from the model indicate that the heat-transfer resistance occurring in the evaporator is the primary factor affecting the total temperature drop in the heat sink embedded with a thermosyphon. Although the effect of vapor flow on the condensation heat transfer can be neglected, the condensation heat transfer in the condenser significantly depends on the type of working fluid. In addition, a new relationship between heat transfer and flow characteristics in terms of the Colburn j_H factor and the Reynolds number was developed to predict the forced airflow effect on the heat-transfer performance of fin-tube condenser, and a correlation for boiling heat transfer occurring in the evaporator was determined experimentally. To verify the prediction, an experimental investigation was conducted to measure the temperature drops from the evaporator to the forced airflow. The experimental results were compared with the theoretical results, and it was found that the theoretical results agree well with the experimental data.

References

[1]Cohen, H., and Bayley, F. J., "Heat-Transfer Problems of Liquid-Cooled Gas-Turbine Blades," *Proceedings of Institution of Mechanical Engineers*, Vol. 169, No. 4, 1955, pp. 1063–1080.

[2]Long, E. L., "The Long Thermopile," *Proceedings of the Permafrost International Conference*, edited by K. B. Woods, National Academy of Sciences–National Research Council, Washington, DC, 1963, pp. 487–491.

[3]Vasiliev, L. L., Vaaz, S. L., Grakovich, L. P., and Sedelkin, V. M., "Heat Transfer Studies for Heat Pipe Cooling and Freezing of Ground," *Advances in Heat Pipe Technology*, edited by D. A. Reay, Pergamon, Oxford, England, U.K., 1981, pp. 63–71.

[4]Faghri, A., *Heat Pipe Science and Technology*, Taylor & Francis, Washington, DC, 1995, pp. 51–53.

[5]Tanaka, O., Yamakaga, H., Ogushi, T., Murakami, M., and Tanaka, Y., "Snow Melting Using Heat Pipe," *Advances in Heat Pipe Technology*, edited by D. A. Reay, Pergamon, Oxford, England, U.K., 1981, pp. 11–23.

[6]Lee, A., and Bedrossian, A., "The Characteristics of Heat Exchangers Using Heat Pipes or Thermosyphons," *International Journal of Heat and Mass Transfer*, Vol. 21, No. 2, 1978, pp. 221–229.

[7]Dunn, P. D., and Reay, D. A., *Heat Pipes*, 4th ed., *Elsevier Science*, New York, 1994, pp. 279–313.

[8]Pande, D. P., Dhar, P. L., Agarwal, R. S., and Amalraj, R. V., "Thermal Hydraulics During Boiling in Thermosyphon Evaporators," *Nuclear Technology*, Vol. 92, No. 2, Nov. 1990, pp. 269–281.

[9]Imura, H., Sasaguchi, K., and Kozai, H., "Critical Heat Flux in a Closed Two-Phase Thermosyphon," *International Journal of Heat and Mass Transfer*, Vol. 26, No. 8, 1983, pp. 1181–1188.

[10]Zuo, Z. J., and Gunnerson, F. S., "Numerical Modeling of the Steady-State Two-Phase Closed Thermosyphon," *International Journal of Heat and Mass Transfer*, Vol. 37, No. 17, 1994, pp. 2715–2722.

[11]Bezrodnyy, M. K., and Elekseyenko, D. V., "Boiling Heat Transfer in Closed Two-Phase Thermosyphons," *Heat Transfer—Soviet Research*, Vol. 9, No. 5, 1977, pp. 14–20.

[12]Gross, U., "Reflux Condensation Heat Transfer Inside a Closed Thermosyphon," *International Journal of Heat and Mass Transfer*, Vol. 35, No. 2, 1992, pp. 279–294.

[13]Nyuyen-Chi, H., and Groll, U., "Entrainment or Flooding Limit in a Closed Two-Phase Thermosyphon," *Proceedings of the 4th International Heat Pipe Conference*, edited by D. A. Reay, Pergamon, Oxford, England, U.K., 1981, pp. 147–162.

[14]Bezrodnyy, M. K., "Flooding of Liquid-Vapor Countercurrent Flow in Closed Thermosyphons," *Heat Transfer—Soviet Research*, Vol. 17, No. 2, 1985, pp. 71–76.

[15]Tien, C. L., and Chung, K. S., "Entrainment Limits in Heat Pipes," *AIAA Journal*, Vol. 17, No. 6, 1978, p. 643.

[16]Shiraishi, M., Yoneya, M., and Yabe, A., "Visual Study of Operating Limit in the Two-Phase Closed Thermosyphon," *Proceedings of the 5th International Heat Pipe Conference*, edited by M. Groll, Vol. 2, Tsukuba Center for Institutes, Tsukuba Science City, Japan, 1984, pp. 10–17.

[17]Andros, F. E., and Florschuetz, L. W., "Heat Transfer Characteristics of the Two-Phase Closed Thermosyphon (Wickless Heat Pipe)," *Proceedings of the 7th International Heat Transfer Conference*, edited by L. L. Vasiler, Vol. 4, General Papers, Begell House, Minsk, Russia, 1982, pp. 187–192.

[18]Harley, C., and Faghri, A., "Complete Transient Two-Dimensional Analysis of Two-Phase Closed Thermosyphons Including the Falling Condensate Film," *Journal of Heat Transfer*, Vol. 116, No. 3, 1994, pp. 418–426.

[19]El-Genk, M. S., and Saber, H. H., "Flooding Limit in Closed, Two-Phase Flow Thermosyphons," *International Journal of Heat and Mass Transfer*, Vol. 40, No. 9, 1997, pp. 2147–2164.

[20]Seban, R. A., and Faghri, A., "Film Condensation in a Vertical Tube with a Closed Top," *International Journal of Heat and Mass Transfer*, Vol. 27, No. 6, 1984, pp. 944–948.

[21]Chen, S. J., Reed, J. G., and Tien, C. L., "Reflux Condensation in a Two-Phase Closed Thermosyphon," *International Journal of Heat and Mass Transfer*, Vol. 27, No. 9, 1984, pp. 1587–1594.

[22]Tien, C. L., Chen, S. L., and Gerner, F. M., "The Wickless Heat Pipe—Two-Phase Closed Thermosyphon," *Experimental Heat Transfer*, Vol. 1, No. 2, 1987, pp. 93–107.

[23]Stuhltrager, E., Miyara, A., and Uehara, H., "Flow Dynamics and Heat Transfer of a Condensate Film on a Vertical Wall—II. Flow Dynamics and Heat Transfer," *International Journal of Heat and Mass Transfer*, Vol. 38, No.15, 1995, pp. 2715–2722.

[24]Miyara, A., "Flow Dynamics and Heat Transfer of Wavy Condensate Film," *Journal of Heat Transfer*, Vol. 123, No. 3, 2001, pp. 492–500.

[25]Zuber, N., "Hydrodynamic Aspects of Boiling Heat Transfer," AEC Rept. AECU-4439, U.S. Government, Washington, DC, 1959.

[26]Tong, L. S., and Tang, Y. S., *Boiling Heat Transfer and Two-Phase Flow*, 2nd ed., Taylor & Francis, Washington, DC, 1997, pp. 40–61.

[27]Rohsenow, W. M., "A Method of Correlating Heat-Transfer Data for Surface Boiling of Liquids," *Journal of Heat Transfer*, Vol. 74, No. 4, 1952, pp. 969–976.

[28]Forster, H. K., and Zuber, N., "Dynamics of Vapor Bubbles and Boiling Heat Transfer," *AIChE Journal*, Vol. 1, No. 4, 1955, p. 531.

[29]Kays, W. M., and London, A. L., *Compact Heat Exchangers*, 2nd ed., McGraw–Hill, New York, 1964, pp. 121–132.

[30]Peterson, G. P., *An Introduction to Heat Pipes, Modeling, Testing and Applications*, Wiley, New York, 1994, pp. 256–258.